Static and Dynamic Event-Triggered Mechanisms for Distributed Secondary Control of Inverters in Low-Voltage Islanded Microgrids

Jianbo Chen, *Graduate Student Member, IEEE*, Dong Yue, *Senior Member, IEEE*, Chunxia Dou, *Member, IEEE*, Shengxuan Weng, Xiangpeng Xie, *Member, IEEE*, Yanman Li, and Gerhard P. Hancke, *Life Fellow, IEEE*

***Abstract*—Due to the high resistance/reactance (R/X) ratio of a low-voltage microgrid (LVMG), virtual complex impedance-based $P - \dot{V}/Q - \omega$ droop control is adopted in this article as the primary control (PC) technique for stabilizing the system. A distributed event-triggered restoration mechanism (ETSM) is proposed as the secondary control (SC) technique to restore the output-voltage frequency and improve power sharing accuracy. The proposed ETSM ensures that neighboring communication happens only at some discrete instants when a predefined event-triggering condition (ETC) is fulfilled. In general, the design of the ETC is the crucial challenge of an event-triggered mechanism (ETM). Thus, in this article, a static ETM (SETM) is proposed as the ETC at first, where two static parameters are utilized to reduce the triggering frequency. Bounded stability is ensured under the SETM, which means that the output-voltage frequency is restored to the vicinity of its nominal value, and close to fair utilization of the distributed generators (DGs) is achieved. To further improve the power sharing accuracy and accelerate the regulation process, a dynamic ETM (DETM) is then introduced. In the DETM, two dynamic parameters that converge to zero in the steady state are designed, which promises asymptotic stability of the system. Besides, Zeno behavior is excluded in both mechanisms. An LVMG consisting of four DGs is constructed in MATLAB/Simulink to illustrate the effectiveness of the proposed methods, and the simulations correspond with our theoretical analysis.**

***Index Terms*—Distributed control, event-triggered mechanism (ETM), microgrid (MG), power sharing, secondary control (SC).**

Manuscript received April 19, 2020; revised June 29, 2020, September 23, 2020, and October 20, 2020; accepted October 25, 2020. This work was supported in part by the National Key Research and Development Program under Grant 2018YFA0702202; in part by the National Natural Science Foundation of China under Grant 61833008, Grant 62073170, and Grant 62022044; in part by the Science and Technology Project of NARI Technology Company Ltd., on "Research on Key Technologies for Simulation and Evaluation of Comprehensive Energy System" under Grant 2019out129; and in part by the Jiangsu Natural Science Foundation for Distinguished Young Scholars under Grant BK20190039. This article was recommended by Associate Editor S. Squartini. *(Corresponding authors: Dong Yue; Chunxia Dou; Gerhard P. Hancke.)*

Jianbo Chen and Dong Yue are with the College of Automation and College of Artificial Intelligence, Nanjing University of Posts and Telecommunications, Nanjing 210023, China (e-mail: jianbo686@aliyun.com; medongy@vip.163.com).

Chunxia Dou, Shengxuan Weng, and Xiangpeng Xie are with the Institute of Advanced Technology, Nanjing University of Posts and Telecommunications, Nanjing 210023, China (e-mail: cxdou@ysu.edu.cn; shxweng@gmail.com; xiexiangpeng1953@163.com).

Yanman Li is with the Branch of Distribution Technology, NARI Technology Company Ltd., Nanjing 211000, China (e-mail: liyanman@sgepri.sgcc.com.cn).

Gerhard P. Hancke is with the School of Automation, Nanjing University of Posts and Telecommunications, Nanjing 210023, China, and also with the Centre for Advanced Sensor Networks, University of Pretoria, Pretoria 0002, South Africa (e-mail: g.hancke@ieee.org).

This article has supplementary material provided by the authors and color versions of one or more figures available at https://doi.org/10.1109/TCYB.2020.3034727.

Digital Object Identifier 10.1109/TCYB.2020.3034727

I. Introduction

With the increasing penetration of distributed generators (DGs), such as photovoltaics (PVs) and wind turbines (WTs), the safe and stable operation of power systems is threatened by the uncontrollable nature of renewable energy (RE). Thus, the microgrid (MG) that integrates DGs, storage systems, and dispersed loads has widely been accepted as a promising candidate to mitigate the side effects of DGs [1], [2].

An MG can operate either in the grid-connected or islanded mode. During the islanded mode, two major requisites are the stability of voltage and current loops and equitable power sharing accuracy among DGs [3]. To fulfil the requirements, various droop methods that emulate the behavior of large synchronous generators [4], [5] have been proposed and well implemented as the primary control (PC) technique. However, since droop control methods introduce a frequency and amplitude (FaA) deviation, a secondary control (SC) action is needed to eliminate the deviation. It should be noted that due to the mismatched feeder impedances, there exists a tradeoff between the power sharing accuracy and voltage regulation [6]. In most existing papers, the accurate power sharing accuracy is preferred at the cost of a larger voltage difference.

Existing SC strategies can be classified into three main classes: 1) centralized SC (CSC) [7], [8]; 2) decentralized SC (DESC) [9], [10]; and 3) distributed SC (DISC) [11]–[16]. Although the CSC architecture is capable of improving the power quality of MGs through the compensation of harmonic and unbalanced components [7], [8], its performance mainly depends on a high-bandwidth communication infrastructure (CI) by which the data of DGs are transmitted to the central controller. Besides, the overall performance of the MG is degraded when any failure, whether in the CI or CSC, occurs [17]. In [9], a generalized washout filter-based

DESC is proposed as a substitution of the PC and SC layer. At the steady state, the output-voltage frequency and magnitude of DGs are restored to their rated value without a CI [10]. However, a CI is required and often constructed in a practical MG because of the requirements of real-time monitoring, economic dispatch, black start and transfer between grid-connected, and islanded modes. Therefore, the DESC architecture has not taken full use of the resources of an MG.

Compared with the CSC and DESC, the DISC architecture has earned worldwide attention for its robustness against time-varying and unreliable communication networks, together with its plug-and-play capability. In [11], the distributed cooperative control strategy of a multiagent system is first adopted in the SC layer. With only neighboring communication between DGs, both the output-voltage frequency and magnitude are restored to its nominal values. As an extension of [11], a distributed finite-time approach is proposed in [12] to accelerate the regulation speed of the SC. In [13], a distributed-averaging proportional-integral (DAPI) frequency controller is proposed at first to restore the system frequency through a thoughtfully designed SC input. Then, a DAPI voltage controller is introduced, where the tradeoff between voltage regulation and reactive power sharing is intuitively presented by tuning of the controller parameters. However, the averaging-based methods may break the system balance during each iteration. Thus, in [16], a set of distributed control laws with dynamic weights is derived from any given communication network. Then, the control laws are utilized to regulate the output of DGs for different targets, which ensures that not only the frequency and magnitude are restored to its nominal value but also the system balance is not broken during iterations.

In the conventional DISC methods [11]–[16], it is assumed that the DGs receive/transmit data continuously or at every sampling time. This assumption requires an ideal CI with sufficient communication resources, which is generally impractical due to the limited bandwidth of a CI [18]–[21]. Therefore, an event-triggered consensus control strategy has been seen as a positive solution to limited resources. In [22], a distributed event-triggered method has been proposed, where a static constant is carefully designed in the event-triggering condition (ETC) to reduce the communication burden. With this method, the system frequency is restored to its nominal value, and fair utilization of DGs is achieved. More importantly, the communication rate has been sharply reduced. Despite these advantages, only bounded stability is ensured, and the tuning of the static parameters is complicated and difficult for a practical MG. In [23], a sampled-data-based event-triggered mechanism (ETM) is proposed for the secondary frequency control. In this method, the ETC is checked only at the sampling instant, and the neighboring communication occurs only when the ETC is violated. Thus, the requirement of the communication resources is remarkably conserved.

Despite numerous SC methods [7]–[16], [22], [23] having proposed, the existing strategies are mainly designed based on the assumption that the output impedances of DGs and feeder impedances are purely inductive, which is not always true, since the output impedance also depends on the control strategy, and the line impedance is predominantly resistive in a low-voltage MG (LVMG)[24]. When the outer voltage and inner current loop of DGs are designed under the $\alpha\beta$ frame and proportional resonant (PR) controllers are adopted, the equivalent output impedance is zero at the fundamental frequency. With the consideration of the resistive nature of an LVMG, it is more appropriate to shape the equivalent impedance between DGs and the point of common coupling (PCC) to be purely resistive through a virtual complex impedance, where a virtual negative inductor is utilized to reduce the effect of the grid-side inductance and a virtual positive resistor is utilized to provide extra damping. Then, a $P-\dot{V}/Q-\omega$ droop method can be adopted as the PC. To the best of our knowledge, an SC strategy based on this application scenario has not been investigated before, especially when the ETM is considered.

Based on the above analysis, a virtual complex impedance-based $P-\dot{V}/Q-\omega$ droop method proposed in [25] is adopted in this study as the PC layer, considering the resistive nature of the LVMG. An ETSM is proposed as the SC strategy to restore the system frequency and improve the power sharing accuracy. To determine the event-triggering instants, both SETM and DETM are then designed as the ETC. In both cases, Zeno behavior is excluded.

The main contributions of this article are summarized as follows.

1) A distributed ETSM is constructed as the SC of the LVMG on the basis of [25]. The proposed ETSM can be seen as a general case of that in [22].
2) An SETM is proposed as the ETC of the DGs. Bounded stability of the closed-loop system is assured and Zeno behavior is excluded under this mechanism. At the steady state, the communication rate is sharply reduced.
3) A DETM is constructed to determine the triggering instants of the DGs. The closed-loop system is asymptotically stable and the transient regulation performance is improved under this mechanism. Besides, the adjacent triggering interval is enlarged during the initial period of load changes, which avoids dense triggering incidents and reduces the requirements on the CI.

The remainder of this article is organized as follows. In Section II, we introduce the models of the LVMG, including the DG, load, and network models. Our control purposes are also pointed out in this section. In Section III, some basic concept of graph theory and ETM are introduced first. Then, we propose the ETSM. Both SETM and DETM are constructed and verified in Section IV. Section V presents simulations to validate our proposed method. Finally, the conclusion is given in Section VI.

II. Problem Formulation

The configuration of a typical LVMG is shown as Fig. 1. There are m DG systems employed in this MG. Each DG system consists of an energy source, an energy storage system, and an inverter with LCL filter. The energy source mainly comprises renewable generators, such as PV and WT, as shown in Fig. 2.

It is assumed that there exist n buses. Buses $1, \ldots, m$ are connected with the DGs and buses $m+1, \ldots, n$ with the public load buses. The DGs can communicate with their neighbors through low-bandwidth communications (LBCs) to fulfil common tasks, such as the secondary voltage and frequency

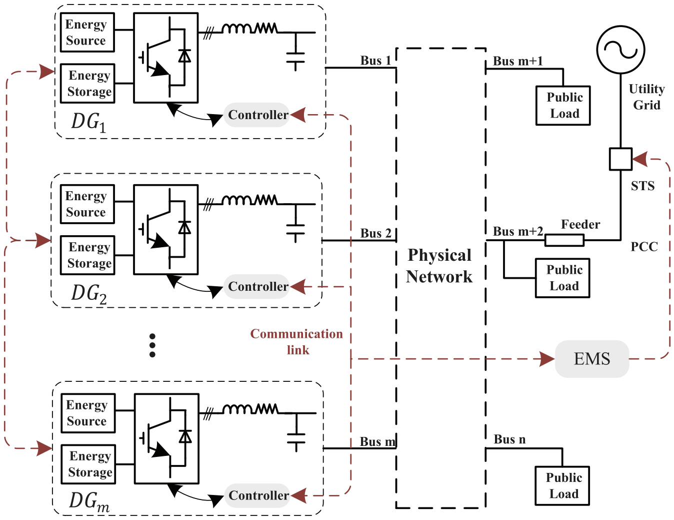

Fig. 1. Configuration of an LVMG.

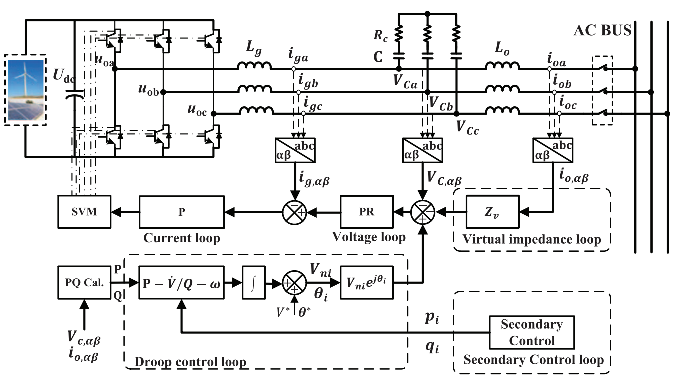

Fig. 2. Hierarchical control of the DG system.

restoration, which is often referred to as the SC [26]. The energy management system (EMS), which functions in the tertiary control (TC) [26], can exchange information with all the DGs to monitor the real-time state of the MG system and ensures economic operation. Besides, the EMS controls the state of the static transfer switch (STS) at the PCC to determine whether the MG operates in the grid-connected or islanded mode. Since only the islanded mode is considered in this study, the centralized control of EMS is ignored.

A. DG Model

The detailed hierarchical control framework of the DG system is shown as Fig. 2. There are five control loops, namely, the outer voltage control loop, inner current control loop, virtual impedance loop, droop control loop, and SC loop. A passive damping strategy is adopted to reduce the resonant peak of the LCL.

Specifically, the DG system is controlled under the $\alpha\beta$ frame, where a PR controller is preferred in the voltage loop for zero steady-state error, and a P controller is utilized in the current loop for the over-current protection and better resonance damping [27]. The virtual impedance consists of a negative inductor and a positive resistor. The virtual negative inductor is adopted to reduce the effect of grid-side inductance, and the virtual positive resistor is utilized to provide extra damping. With the virtual impedance method, the equivalent impedance between DG and PCC is reshaped to be purely resistive. Therefore, the active and reactive power are decoupled, and a traditional $P-V/Q-\omega$ droop equation is able to stabilize the DG system. However, due to the mismatched feeder impedance, the equivalent resistive impedance of DGs may not be equal. In [28] and [29], a $Q-\dot{V}$ droop method was first proposed to improve the reactive power sharing accuracy for the purely inductive case. Inspired by this method, a $P-\dot{V}$ droop method proposed in [25] is adopted in this study to improve the active power sharing accuracy

$$\begin{aligned} D_{pi}\dot{V}_i(t) &= P_i^* - P_i(t) - p_i(t) \\ V_{ni} &= V^* + \int \dot{V}_i(\tau)d\tau \\ D_{qi}\dot{\theta}_i(t) &= -\big(Q_i^* - Q_i(t) - q_i(t)\big) \end{aligned} \tag{1}$$

where the positive constants D_{pi} and D_{qi} are the droop coefficients of DG_i, P_i^*, and Q_i^* are the nominal active and reactive power rating of DG_i, and $p_i(t)$ and $q_i(t)$ are two variables introduced to enhance the active and reactive power sharing accuracy. V_{ni} is the voltage magnitude reference of the voltage controller and $\dot{V}_i(t)$ is the derivative of V_{ni}. θ_i is the phase angle reference and $\dot{\theta}_i(t) = \omega_i(t)$ is the angular frequency reference.

For simplicity, it is assumed that the DGs do not reach their power output limitations. Supposing that the load changes at $t = t_0$ and $p_i(t) = p_i(t_0)$ holds for $t > t_0$, the $\dot{V}$ mechanism will continuously regulate the voltage magnitude until $P_i(t) + p_i(t_0) = P_i^*$. This regulation process not only requires a longer settling time but may also result in the violation of the required voltage level [28]. It is the same case for ω. Therefore, an SC loop is needed to reset $\dot{V}$ and $\dot{\theta}_i(t)$ to zero and restore the system frequency. A decentralized SC method is proposed in [28], as shown in

$$\begin{aligned} \dot{p}_i &= k_{\text{pri}}\dot{V}_i(t) \\ \dot{q}_i &= -k_{\text{qri}}\dot{\theta}_i(t) \end{aligned} \tag{2}$$

where k_{pri} and k_{qri} are the restoration coefficients, which regulate the speed of the dynamic restoration process.

With the proper design of k_{pri} and k_{qri}, both the voltage magnitude and frequency are restricted to an allowable range after $\dot{\theta}_i$ and $\dot{V}$ are reset to zero. Since the main contributions of this study lie in the SC layer, a more detailed discussion about the $P-\dot{V}$ droop method is omitted here and can be found in [25].

Remark 1: k_{pri} and k_{qri} must be carefully chosen to achieve a balance between the sharing accuracy, voltage level, and settling time [28]. For example, if k_{pri} is a large quantity, the dynamic regulation takes less time to reach the steady state. However, the sharing accuracy deteriorates and the voltage level may break the required operation code. If k_{pri} is chosen small, both the sharing accuracy and voltage level are fulfilled at the cost of longer regulation time.

Remark 2: Since the initial $p_i(0)$ and regulation process of DG_i are different, $p_i(t)/D_{pi} \neq p_j(t)/D_{pj}$ and $P_i(t)/D_{pi} \neq$

$P_j(t)/D_{pj}$ hold at the steady state, which means the active power cannot be shared proportionally under the $P-\dot{V}/Q-\omega$ droop method [29]. Nevertheless, the sharing accuracy under the $P-\dot{V}$ droop method has been improved compared with the traditional $P-V$ droop method [25], [28].

B. Network Model

The overall active and reactive power flows P_i and Q_i at node i for $i = 1, \ldots, m$ are given by [30]

$$\begin{aligned} P_i &= \sum_{j=1}^{n} V_i V_j (G_{ij}\cos\delta_{ij} + B_{ij}\sin\delta_{ij}) \\ Q_i &= \sum_{j=1}^{n} V_i V_j (G_{ij}\sin\delta_{ij} - B_{ij}\cos\delta_{ij}) \end{aligned} \tag{3}$$

where G_{ij}, B_{ij}, and δ_{ij} are the conductance, susceptance, and power angle between node i and node j, respectively.

In this study, the line impedance of the LVMG is modeled to be resistive. Thus, the active and reactive power flows, P_i and Q_i, are simplified as

$$\begin{aligned} P_i &= \sum_{j=1}^{n} G_{ij} V_i V_j \cos(\delta_{ij}) \\ Q_i &= \sum_{j=1}^{n} G_{ij} V_i V_j \sin(\delta_{ij}). \end{aligned} \tag{4}$$

C. Load Model

The structure-preserving model is adopted to model the constant power flows P_{Li} and Q_{Li} at load $i \in \{m+1, \ldots, n\}$ [22], [30]

$$\begin{aligned} D_{Lpi}\dot{\theta}_i(t) &= -P_{Li} - P_i(t) \\ D_{Lqi}\dot{V}_i(t) &= -Q_{Li} - Q_i(t) \end{aligned} \tag{5}$$

where D_{Lpi} and D_{Lqi} are sufficiently small positive constants.

D. Control Purpose

The DG, network and load models (1), (2), (4), (5) are combined to be the frequency control and power sharing model of the isolated LVMG of this article.

According to Remark 2, the proportional sharing accuracy cannot be achieved under the $P-\dot{V}$ droop method. However, it should be noted that the restoration mechanism (2) is implemented in DGs separately. Thus, it is reasonable to incorporate communication links between DGs to avoid the drawbacks of (2) [30]. With an appropriate consensus strategy, $p_i(t)/D_{pi} = p_j(t)/D_{pj}$, $q_i(t)/D_{qi} = q_j(t)/D_{qj}$, and $P_i(t)/D_{pi} = P_j(t)/D_{pj}$, $Q_i(t)/D_{qi} = Q_j(t)/D_{qj}$ for $i, j = 1, \ldots, m$ can be fulfilled, which means the proportional sharing accuracy can be achieved. Besides, the parameter selection of k_{pri} and k_{qri} can be simplified [30].

In addition to the theoretical results, we also pay attention to the practical implementation of the proposed methods. Considering the limited resources of the CI, the communication rate of the consensus strategy candidates cannot be extremely high.

In conclusion, our control purposes can be summarized as follows.

Purpose 1: Restore the system frequency to an arbitrary small neighborhood of its nominal value, which means $|\omega_i - \omega^*| \le C_\omega$ holds for $i = 1, \ldots, m$. Besides, $|P_i^* - P_i(t) - p_i(t)| \le C_{pi}$ and $|Q_i^* - Q_i(t) - q_i(t)| \le C_{qi}$ holds for $i = 1, \ldots, m$, $P_{Li} + P_i(t) \equiv 0$ and $Q_{Li} + Q_i(t) \equiv 0$ for load $i = m+1, \ldots, n$ at the steady state. C_ω, C_{pi}, and C_{qi} are small positive constants used to lower the communication rate.

Purpose 2: Realize the proportional active and reactive power sharing. This purpose is mathematically described as $|P_i(t)/P_i^* - P_j(t)/P_j^*| \le C_{Pi}$ and $|Q_i(t)/Q_i^* - Q_j(t)/Q_j^*| \le C_{Qi}$ for $i, j = 1, \ldots, m$ at steady state. C_{Pi} and C_{Qi} are small constants used to lower the communication rate.

Purpose 3: Reduce the communication rate to a realizable level, especially exclude Zeno behavior. The Zeno behavior happens if there exists an accumulation point of the event times. In other words, an infinite number of events occur within a finite-time interval [31]. This purpose is mandatory for the proposed consensus strategy to be practical.

It should be mentioned that reducing the communication rate and avoiding Zeno behavior are not invariably linked. They are required in purpose 3 with the consideration that the ETM is introduced in the following sections. Besides, small values of C_{pi}, C_{qi}, C_{Pi}, and C_{Qi} are acceptable, since in a practical MG, both voltage, and frequency are allowed to fluctuate in a predefined scope [22].

III. Proposed Event-Triggered Restoration Mechanism

Since the following proposed control strategies are based on the multiagent consensus method and ETM, some preliminary concepts of the graph theory [12] and ETM are briefly presented at first. Then, an ETSM is proposed to fulfil the three purposes mentioned in Section II-D.

A. Basic Graph Theory

An undirected connected graph is denoted as $\mathcal{G} = (\mathcal{V}, \xi)$, where $\mathcal{V} \triangleq \{\nu_1, \nu_2, \ldots, \nu_m\}$ is the node set, and $\xi \triangleq \{(\nu_j, \nu_i), if\, j \to i\}$ is the edge set, where $j \to i$ denotes that node i can receive information from node j. The set of neighbors of node i is denoted as $N_i \triangleq \{\nu_j \in \mathcal{V} | (\nu_j, \nu_i) \in \xi\}$, whose cardinal number is $|N_i|$. The Laplacian matrix of $\mathcal{G}$ is defined as $L \triangleq \{l_{ij}\} \in R^{m\times m}$, where $l_{ij} = -1$ if and only if $(i, j) \in \xi$, otherwise, $l_{ij} = 0$ and $l_{ii} = -\sum_{j\neq i} l_{ij}$.

B. Basic Concept of the Event-Triggered Mechanism

For a multiagent system consisting of n agents, there are two common ways to identify the instants when agent i should transmit its information to its neighbors: 1) periodic time-triggered mechanism (PTTM) and 2) ETM. The simplified communication mechanisms of a multiagent system are shown as Fig. 3.

Taking agent 1 as an example, the information of its neighbors is transmitted through the communication network to its controller. If no more information arrives, the last received one will be seen as the newest data utilized in the controller

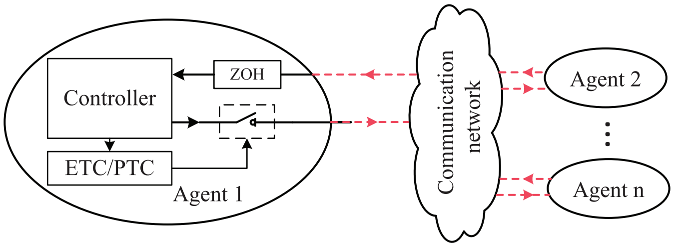

Fig. 3. Communication mechanism: PTTM and ETM.

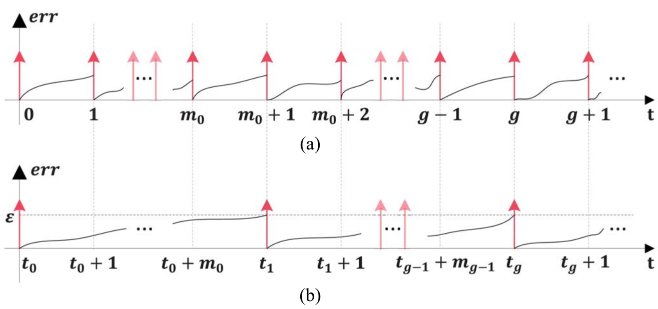

Fig. 4. Comparison of triggering instants. (a) PTTM. (b) ETM.

due to the zero-order hold (ZOH) method. The PTTM means that the local data of agent 1 are transmitted to its neighbors every predefined time interval, for example, the sampling period T_s. The corresponding condition is named as the periodic triggering condition (PTC). The ETM denotes that the local information is transferred to its neighbors only when the predefined ETC is fulfilled.

To illustrate the difference between the PTTM and ETM, the triggering instants of both mechanisms, which are represented by red arrows, are shown in Fig. 4, where the light red arrows denote several triggering instants between red arrows. The black curve denotes the error defined in (6). For simplicity, g and m_o are short for $g * T_s$, $m_o * T_s$, where $g, m_o \in \mathbb{N}$.

Supposing that the measurement error of agent i is defined as

$$e_i(t) = x_i(t) - x_i(t_g^i) \tag{6}$$

where $x_i(t)$ denotes the present state of agent i, and $x_i(t_g^i)$ denotes the newest triggering state at the triggering instant t_g^i.

As for the PTTM, t_g^i is always equal to the latest sampling instant. Therefore, e_i is reset to zero at every sampling instant as shown in Fig. 4(a). Under this mechanism, the time t can be split as a combination of successive sampling instants and is formulated as $t = [0, 1) \cup [1, 2) \cup \cdots [g-1, g) \cup [g, g+1) \cup \cdots = [0, +\infty)$.

Different from the PTTM, t_g^i is updated only when the predefined ETC, for example, $e_i^2(t) > \varepsilon$, is fulfilled. In general, the design of ε is the core of an ETC. In Fig. 4(b), ε is chosen as a constant for illustration. Under the ETM, the time t is arranged as a combination of successive triggering instants and is formulated as $t = [t_0^i, t_1^i) \cup [t_1^i, t_2^i) \cup \cdots [t_{g-1}^i, t_g^i) \cup [t_g^i, t_{g+1}^i) \cup \cdots = [0, +\infty)$, where $[t_g^i, t_{g+1}^i) = [t_g^i, t_g^i + 1) \cup [t_g^i + 1, t_g^i + 2) \cup \cdots \cup [t_g^i + m_g, t_{g+1}^i)$.

C. Proposed Event-Triggered Restoration Mechanism

To achieve the three purposes proposed in Section II-D, the restoration mechanism (2) is replaced by the proposed distributed event-triggered restoration mechanism (ETSM) (7).

Event-Triggered Restoration Mechanism:

$$\begin{aligned} k_{pi}\dot{p}_i(t) &= P_i^* - P_i(t) - p_i(t) \\ &\quad + \lambda_{pi} \sum_{j \in N_i} \left(\frac{p_j(t_{g'(t)}^j)}{D_{pj}} - \frac{p_i(t_g^i)}{D_{pi}} \right), \ t \in \left[t_g^i, t_{g+1}^i\right) \\ k_{qi}\dot{q}_i(t) &= Q_i^* - Q_i(t) - q_i(t) \\ &\quad + \lambda_{qi} \sum_{j \in N_i} \left(\frac{q_j(\tau_{h'(t)}^j)}{D_{qj}} - \frac{q_i(\tau_h^i)}{D_{qi}} \right), \ t \in \left[\tau_h^i, \tau_{h+1}^i\right) \end{aligned} \tag{7}$$

where $k_{pi} = D_{pi}/k_{\text{pri}}$ and $k_{qi} = D_{qi}/k_{\text{qri}}$. $\lambda_{pi,qi}$ determine the influence of sharing accuracy on the restoration process. $t_{g'(t)}^j$ and $\tau_{h'(t)}^j$ are the newest triggering instants corresponding to $p_j(t)$ and $q_j(t)$ of DG$_j$. t_g^i and τ_h^i are the latest triggering instants related to $p_i(t)$ and $q_i(t)$ of DG$_i$.

As for DG$_i$, (7) shows that only the local information and latest triggering states, $p_j(t_{g'(t)}^j)$ and $q_j(\tau_{h'(t)}^j)$ for $j \in N_i$, are needed to implement the ETSM. During two successive triggering instants of DG$_j$, for example, $t \in [t_{g'(t)}^j, t_{g'(t)+1}^j)$, the real-time state of DG$_j$ will not be transmitted to DG$_i$ as analyzed in Section III-B.

The difference between (2) and (7) is that (2) is implemented in a decentralized way while (7) in a distributed way. With the neighboring information exchange, the proposed ETSM is able to restore the frequency and further improve the power sharing accuracy [22]. Besides, the introduction of ETM can reduce the requirement on the CI.

Remark 3: The parameters k_{pri} and k_{qri} are assumed to be one in [22], while they are utilized to regulate the restoration speed of the ETSM in this research. The parameters λ_{pi} and λ_{qi} are chosen to be one in [22] and [30]. However, due to the effect of droop coefficients $(1/D_{pi})$ and $(1/D_{pj})$, the influence of the power sharing difference, $p_j(t_{g'(t)}^j) - p_i(t_g^i)$ and $q_j(\tau_{h'(t)}^j) - q_i(\tau_h^i)$, on the restoration process is heavily weakened. The distributed mechanism might degrade into a decentralized method when $\sum_{j \in N_i}(([p_j(t_{g'(t)}^j)]/D_{pj}) - ([p_i(t_g^i)]/D_{pi}))$ is neglectable compared with $P_i^* - P_i(t) - p_i(t)$. Therefore, λ should be carefully tuned, and the proposed ETSM can be seen as an improved case of that in [22] and [30].

IV. Proposed Event-Triggered Mechanism

For the closed-loop system constructed by (1), (4), (5) and (7), although the ETSM has been proposed, an ETC of DG$_i$ for $i = 1, \ldots, m$ is still required to determine the triggering instants $\{t_g^i\}_{g=0}^{\infty}$ and $\{\tau_h^i\}_{h=0}^{\infty}$.

In this section, an SETM is proposed at first to fulfil the three purposes noted in Section II-D. Then, a DETM is also given. The differences between the SETM and DETM are summarized at the end of this section.

A. Static Distributed Event-Triggered Mechanism

The measurement errors of DG_i with respect to $p_i(t)$ and $q_i(t)$ are defined as

$$\begin{aligned} e_{pi}(t) &= p_i(t) - p_i(t_g^i), \quad t \in \left[t_g^i, t_{g+1}^i\right) \\ e_{qi}(t) &= q_i(t) - q_i(\tau_h^i), \quad t \in \left[\tau_h^i, \tau_{h+1}^i\right). \end{aligned} \tag{8}$$

The SETM of DG_i for $i \in \{1, \ldots, m\}$ is designed as follows.

Static ETM (SETM):

The ETC of DG_i is constructed as

$$\begin{aligned} e_{pi}^2(t) > &\sum_{j\in N_i} \frac{D_{pi}^2}{4|N_i|}\left(\frac{p_j(t^i_{g'(t)})}{D_{pj}} - \frac{p_i(t_g^i)}{D_{pi}}\right)^2 \\ &+ \frac{D_{pi}\left(P_i^* - P_i(t) - p_i(t)\right)^2}{2\lambda k_{pr} V_i |N_i|} + \frac{D_{pi}^2}{\lambda k_{pr}|N_i|}\eta_{pi} \\ e_{qi}^2(t) > &\sum_{j\in N_i} \frac{D_{qi}^2}{4|N_i|}\left(\frac{q_j(\tau^j_{h'(t)})}{D_{qj}} - \frac{q_i(\tau_h^i)}{D_{qi}}\right)^2 \\ &+ \frac{D_{qi}(Q_i^* - Q_i(t) - q_i(t))^2}{2\lambda k_{qr}|N_i|} + \frac{D_{qi}^2}{\lambda k_{qr}|N_i|}\eta_{qi} \end{aligned} \tag{9}$$

where $|N_i|$ is the number of neighbors of DG_i. η_{pi} and η_{qi}, which represent the static quantities within the SETM, are positive constants. Besides, $\lambda_{pi} = \lambda_{qi} = \lambda$, $k_{\mathrm{pri}} = k_{prj} = k_{pr}$, and $k_{\mathrm{qri}} = k_{qrj} = k_{qr}$ are chosen deliberately.

The right-hand side of the inequalities can be seen as a changing threshold ε mentioned in Section III-B. Only when any of the inequalities holds, the communication function is activated, and the local data, $p_i(t_{g+1}^i)$ and $q_i(\tau_{h+1}^i)$, are transmitted to the neighbors of DG_i for $i = 1, \ldots, m$. In other words, the ETC (9) determines the triggering instants $\{t_g^i\}_{g=0}^{\infty}$ and $\{\tau_h^i\}_{h=0}^{\infty}$. The capacitor voltage V_i in the ETC corresponding to $p_i(t)$ represents the coupling of voltage magnitude V and active power P in the LVMG, which is different from that in [22].

Theorem 1: The restoration mechanism (7) with SETM (9) restores the frequency into an arbitrary small neighborhood of nominal value, i.e., $|\omega_i - \omega^*| \leq C_\omega$. Besides, $|P_i^* - P_i(t) - p_i(t)| \leq C_{pi}$ and $|Q_i^* - Q_i(t) - q_i(t)| \leq C_{qi}$ hold for $i = 1, \ldots, m$, where C_ω, C_{pi}, and C_{qi} are arbitrary small positive constants. The utilization ratio of all energy sources achieves bounded consensus, i.e., $|P_i(t)/P_i^* - P_j(t)/P_j^*| \leq C_{Pi}$ and $|Q_i(t)/Q_i^* - Q_j(t)/Q_j^*| \leq C_{Qi}$ for $i, j = 1, \ldots, m$ at steady state, where $C_{Pi} = (2D_{pi}/P_i^*\sqrt{\lambda k_{pr}} + \sqrt{2D_{pi}V_i}/P_i^* + \sqrt{2D_{pj}V_j}/P_j^*)\eta'$, $C_{Qi} = (2D_{qi}/Q_i^*\sqrt{\lambda k_{qr}} + \sqrt{2D_{qi}}/Q_i^* + \sqrt{2D_{qj}}/Q_j^*)\eta'$ and $\eta' = \sqrt{\sum_{i=1}^m (\eta_{pi} + \eta_{qi})}$.

Proof: See the supplementary materials. ∎

Theorem 1 promises that purposes 1 and 2 can be fulfilled by (7) and (9). In other words, the system frequency is restored to the neighborhood of its nominal value, and nearly fair utilization of DGs is achieved.

To satisfy purpose 3, Theorem 2 is given to determine the upper bound of the communication rate, which is equivalent to the lower bound of the adjacent time intervals of the triggering mechanism (9).

Theorem 2: The lower bounds of the successive triggering time intervals for the ETC (9) are described as

$$\begin{aligned} t_{g+1}^i - t_g^i > &\frac{1}{M_{pi}}\left(\sum_{j\in N_i} \frac{D_{pi}^2}{4|N_i|}\left(\frac{p_j(t^j_{g'(t^i_{g+1})})}{D_{pj}} - \frac{p_i(t_g^i)}{D_{pi}}\right)^2\right. \\ &+ \frac{D_{pi}\left(P_i^* - P_i(t_{g+1}^i) - p_i(t_{g+1}^i)\right)^2}{2\lambda k_{pr} V_i |N_i|} \\ &\left. + \frac{D_{pi}^2}{\lambda k_{pr}|N_i|}\eta_{pi}\right)^{\frac{1}{2}} \\ \tau_{h+1}^i - \tau_h^i > &\frac{1}{M_{qi}}\left(\sum_{j\in N_i} \frac{D_{qi}^2}{4|N_i|}\left(\frac{q_j(\tau^j_{h'(\tau^j_{h+1})})}{D_{qj}} - \frac{q_i(\tau_h^i)}{D_{qi}}\right)^2\right. \\ &+ \frac{D_{qi}(Q_i^* - Q_i(\tau_{h+1}^j) - q_i(\tau_{h+1}^j))^2}{2\lambda k_{qr}|N_i|} \\ &\left. + \frac{D_{qi}^2}{\lambda k_{qr}|N_i|}\eta_{qi}\right)^{\frac{1}{2}} \end{aligned} \tag{10}$$

where M_{pi} and M_{qi} are positive constants.

Proof: See the supplementary materials. ∎

Remark 4: Equation (10) promises that $t_{g+1}^i - t_g^i > 1/M_{pi}(D_{pi}^2/\lambda k_{pr}|N_i|\eta_{pi})^{1/2}$ and $\tau_{h+1}^i - \tau_h^i > 1/M_{qi}(D_{qi}^2/\lambda k_{qr} |N_i|\eta_{qi})^{1/2}$, which means that the Zeno behavior is avoided. The minimum adjacent time interval can be regulated by predefined static parameters η_{pi} and η_{qi}. The larger η_{pi} and η_{qi} are, the lower the triggering rate will be. However, $|P_i(t)/P_i^* - P_j(t)/P_j^*|$ and $|Q_i(t)/Q_i^* - Q_j(t)/Q_j^*|$ will fluctuate in a larger bound since C_{Pi} and C_{qi} are positive correlated with η_{pi} and η_{qi}. The power sharing accuracy can be improved by decreasing η_{pi} and η_{qi} at the cost of higher communication rate, especially when the load changes. Therefore, there exists a tradeoff between the control precision and communication bandwidth.

Remark 5: In spite of the aforementioned tradeoff, purposes 1–3 can be fulfilled by the SETM with ETSM, and the bounded stability of the system can be ensured. Thus, the proposed SETM with ETSM outperforms the traditional $P - \dot{V}/Q - \omega$ droop method with respect to frequency restoration and power sharing accuracy. Moreover, the adoption of the ETM can reduce the communication burden and ensure that the proposed SETM is more practical than the method in [30], which requires continuous information exchange.

B. Dynamic Distributed Event-Triggered Mechanism

The tradeoff of the SETM (9) inspired the authors to design another mechanism that can not only reduce the triggering frequency when the load changes but also guarantee the asymptotical convergence of the power sharing accuracy. Thus, purposes 1 and 2 are modified as follows.

Purpose 4: The same requirements as purpose 1 except for $C_\omega = 0$, $C_{pi} = 0$, and $C_{qi} = 0$.

Purpose 5: The same requirements as purpose 2 except for $C_{Pi} = 0$ and $C_{Qi} = 0$.

In this section, we propose the following DETM to fulfil purposes 3–5.

Dynamic ETM (DETM):

The ETC of DG_i is designed as

$$
\begin{aligned}
e_{pi}^2(t) > \alpha_{pi}\Bigg(&\sum_{j\in N_i}\frac{D_{pi}^2}{4|N_i|}\left(\frac{p_j(t^j_{g'(t)})}{D_{pj}}-\frac{p_i(t^i_g)}{D_{pi}}\right)^2\\
&+\frac{D_{pi}\left(P_i^*-P_i(t)-p_i(t)\right)^2}{2\lambda k_{pr}V_i|N_i|}+\frac{D_{pi}^2}{\lambda k_{pr}|N_i|}\varphi_{pi}(t)\Bigg)\\
e_{qi}^2(t) > \alpha_{qi}\Bigg(&\sum_{j\in N_i}\frac{D_{qi}^2}{4|N_i|}\left(\frac{q_j(\tau^j_{h'(t)})}{D_{qj}}-\frac{q_i(\tau^i_h)}{D_{qi}}\right)^2\\
&+\frac{D_{qi}\left(Q_i^*-Q_i(t)-q_i(t)\right)^2}{2\lambda k_{qr}|N_i|}+\frac{D_{qi}^2}{\lambda k_{qr}|N_i|}\varphi_{qi}(t)\Bigg)
\end{aligned}
\tag{11}
$$

where α_{pi} and α_{qi} are positive constant variables, and $\varphi_{pi}(t)$ and $\varphi_{qi}(t)$ are the internal dynamic variables. The dynamic regulation of $\varphi_{pi}(t)$ and $\varphi_{qi}(t)$ is constructed as

$$
\begin{aligned}
&\dot{\varphi}_{pi}(t)\\
&= -\beta_{pi}\varphi_{pi}(t)+\gamma_{pi}\Bigg(\sum_{j\in N_i}\frac{\alpha_{pi}D_{pi}^2}{4|N_i|}\left(\frac{p_j(t^j_{g'(t)})}{D_{pj}}-\frac{p_i(t^i_g)}{D_{pi}}\right)^2\\
&\quad+\frac{\alpha_{pi}D_{pi}}{2\lambda k_{pr}V_i|N_i|}\left(P_i^*-P_i(t)-p_i(t)\right)^2-e_{pi}^2(t)\Bigg)\\
&\dot{\varphi}_{qi}(t)\\
&= -\beta_{qi}\varphi_{qi}(t)+\gamma_{qi}\Bigg(\sum_{j\in N_i}\frac{\alpha_{qi}D_{qi}^2}{4|N_i|}\left(\frac{q_j(\tau^j_{h'(t)})}{D_{qj}}-\frac{q_i(\tau^i_h)}{D_{qi}}\right)^2\\
&\quad+\frac{\alpha_{qi}D_{qi}}{2\lambda k_{qr}|N_i|}\left(Q_i^*-Q_i(t)-q_i(t)\right)^2-e_{qi}^2(t)\Bigg)
\end{aligned}
\tag{12}
$$

where β_{pi}, β_{qi}, γ_{pi}, and γ_{qi} are all positive constant variables, $\varphi_{pi}(0) \geq 0$, $\varphi_{qi}(0) \geq 0$ and the following inequalities hold:

$$
\begin{aligned}
&\alpha_{pi} \leq (\lambda k_{pr}|N_i|)/(\lambda k_{pr}|N_i| + \gamma_{pi}D_{pi}^2)\\
&\alpha_{qi} \leq (\lambda k_{qr}|N_i|)/(\lambda k_{qr}|N_i| + \gamma_{qi}D_{qi}^2)\\
&\alpha_{pi} \leq \beta_{pi}, \alpha_{qi} \leq \beta_{qi}
\end{aligned}
\tag{13}
$$

where α_{pi} and α_{qi} are deliberately introduced for convenience of proof. Equation (13) shows that $\alpha_{pi}, \alpha_{qi} \leq 1$.

Remark 6: $\lim_{t\to\infty}\dot{\varphi}_{pi}(t) = 0$, $\lim_{t\to\infty}\dot{\varphi}_{qi}(t) = 0$ and $\lim_{t\to\infty}\varphi_{pi}(t) = \delta_{fp}/\beta_{pi}$, $\lim_{t\to\infty}\varphi_{qi}(t) = \delta_{fq}/\beta_{qi}$ hold at the steady state, where δ_{fp} and δ_{fq} are sufficient small positive values owing to the asymptotical stability. A small disturbance of P_i/Q_i will activate DG_i to transmit its information to its neighbors. Thus, the triggering frequency of (9) is smaller than that of (11) at the steady state. However, at the initial load variation, the difference between $p_j(t^j_{g'(t)})$, $q_j(\tau^j_{h'(t)})$, and $p_i(t^i_g)$, $q_i(\tau^i_h)$ may be enlarged, respectively, making φ_{pi} and φ_{qi} to increase to a larger quantity compared with η_{pi} and η_{qi}. Therefore, the triggering frequency of (11) is smaller compared with that of (9) during the transient state.

Theorem 3: The restoration mechanism (7) with DETM (11), (12) restores the frequency to its nominal value at steady state, i.e., $\omega_i = \omega^*$. Besides, $P_i^* - P_i(t) - p_i(t) \equiv 0$ and $Q_i^* - Q_i(t) - q_i(t) \equiv 0$ holds for $i = 1, \ldots, m$. The accurate fair utilization of all energy sources is realized, i.e., $P_i(t)/P_i^* = P_j(t)/P_j^*$ and $Q_i(t)/Q_i^* = Q_j(t)/Q_j^*$ for $i, j = 1, \ldots, m$ at steady state.

Proof: See the supplementary materials. ■

Theorem 3 indicates that the system is asymptotically stable and the accurate, fair utilization of DGs is ensured. Thus, purposes 4 and 5 can be fulfilled by the proposed DETM with ETSM. For completeness, the following theorem is presented to verify the exclusion of Zeno behavior.

Theorem 4: With the dynamic distributed ETM (11) and (12), the Zeno behavior is excluded.

Proof: See the supplementary materials. ■

With Theorems 3 and 4, our purposes 3–5 can be fulfilled.

C. Comparison of Static and Dynamic Event-Triggered Mechanism

Although both SETM and DETM can fulfil our requirements, restoring the frequency and improving the power sharing accuracy while reducing the communication burden, both have their own pros and cons.

As for the SETM, its pros are as follows.

1) Only one pair of constant parameters, η_{pi} and η_{qi}, is required to be designed, while three pairs of parameters need to be selected for the DETM.
2) At the steady state, the triggering interval is larger with the adoption of η_{pi} and η_{qi}, which reduces the communication burden.
3) Bounded stability of the system is ensured and the Zeno behavior is excluded as verified by Theorems 1 and 2.

Its cons are as follows.

1) The selection of η_{pi} and η_{qi} is complicated since there exists a tradeoff between the sharing accuracy and communication burden. In most cases, it requires trial and error.

The pros of the DETM are as follows.

1) The selection of α_{pi}, α_{qi}, β_{pi}, β_{qi}, γ_{pi}, and γ_{qi} is much easier than η_{pi} and η_{qi} due to the incorporation of internal dynamic variables φ_{pi} and φ_{qi} as shown in Table I.
2) With the dynamic regulation of φ_{pi} and φ_{qi}, the triggering frequency is reduced when the load changes according to Remark 6.
3) The system is asymptotically stable and the Zeno behavior is excluded as proved by Theorems 3 and 4.

Its cons are as follows.

1) The dynamic regulation of φ_{pi} and φ_{qi} increases the computation complexity of the DETM.
2) Since φ_{pi} and φ_{qi} are reset to zeros, the triggering frequency of the DETM is relatively higher than that of the SETM at the steady state.

In conclusion, both SETM and DETM are suitable candidates to restore the frequency and improve the power sharing accuracy. The adoption of either should cater for the application scenario.

D. Comparison With Previously Reported Method [21]

A robust secondary frequency controller based on a dynamic ETM has been examined in [21] to cope with the uncertainty of RE and to reduce the communication burden. The differences between our method and the one in [21] are listed as follows.

1) The control object is different. Our work concentrates on the secondary frequency control and the power sharing accuracy while Yang's paper only concentrates on the robust secondary frequency control.
2) The mathematical model is different. On the basis of our previous work [25], the detailed model of the inverter is presented, while the RE generators are described by first-order lag transfer functions in Yang's paper.
3) The experimental setup is different. Our MG consists of only four inverters, while Yang's MG incorporates a synchronous generator, which provides the voltage and frequency support.

Therefore, our method and that in [21] are two algorithms designed for different types of islanded AC MG.

V. Simulations

In order to demonstrate the effectiveness of the proposed distributed ETSM (7) and ETM (9), (11), (12), an islanded LVMG has been constructed in the MATLAB/Simulink platform. As shown in Fig. 5, there are four DGs considered in this LVMG. DG_1 and DG_4 are connected to a local load, respectively. The complex impedances Z_{12}, Z_{23}, and Z_{34} represent the line impedance between DGs. The neighboring communication is denoted by red arrows, as illustrated in Fig. 5. The detailed parameters of the experimental setup are listed in Table I. The simulations of the PTTM are also discussed for comparison.

A. Case Study: Static Event-Triggered Mechanism

The whole regulation process is shown as Figs. 6 and 7. At the start of the simulation, only DG_1 is activated as a grid-forming inverter and injects the active and reactive power consumed by the load 1, 2. At $t = 0.3$ s, $DG_{2,3,4}$ are enabled. Then, they are synchronized with DG_1 through a phase-locked loop (PLL) and connected to DG_1 at $t = 0.5$ s. Between $t = 0.5$ and 1.8 s, the DGs are controlled under the traditional $P - V/Q - \omega$ droop method. At $t = 1.8$ s, the ETSM with SETM is activated. Load 1 is suddenly cut off at $t = 20$ s, and then reconnected at $t = 40$ s.

According to Fig. 6(a), the active power injections of DGs at $t = 1.8$ s are $P_1 = 4.82$ KW, $P_2 = 4.3$ KW, $P_3 = 4.2$ KW, and $P_4 = 4.22$ KW, respectively. The proportion of P_3 to P_1 is 87.14%, which means that the fair utilization of DGs is not achieved under the $P - V$ droop method. Since the SETM is activated at $t = 1.8$ s, the active power sharing difference begin to decrease. At $t = 20$ s, the power sharing accuracy has been improved to $(P_4/P_1) = 97.78\%$. When the load is disconnected at $t = 20$ s, the enlarged initial power sharing difference due to the line impedances can still be diminished, which illustrates the robustness of the proposed SETM against load changes. After regulation, the proportion of P_1–P_4 is 98.43% at $t = 40$ s. Thus, compared with the $P - V/Q - \omega$

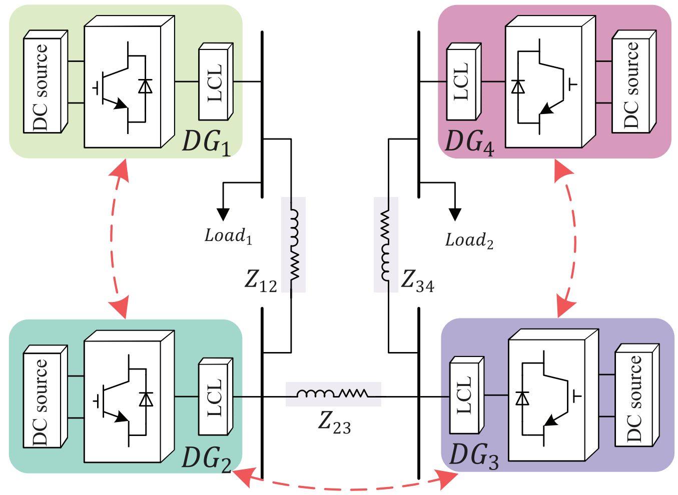

Fig. 5. Schematic of the experimental LVMG setup.

TABLE I
Electrical and Control Parameters

Electrical parameters		
Parameter	symbol	Value
Nominal Frequency	f^*	50Hz
Sampling Frequency	f_s	20kHz
DC Voltage	V_{dc}	700V
Nominal Voltage	V^*	311V
Filter Inductance	L_g	1mH
Filter Capacitance	C	15uF
Passive Resistance	R_c	1.6Ω
Line Impedance (1,2)	Z_{12}	R=0.4Ω,L=10uH
Line Impedance (2,3)	Z_{23}	R=0.1Ω,L=50uH
Line Impedance (3,4)	Z_{34}	R=0.8Ω,L=40uH
Control parameters		
Rated Active Power	P_i^*	10KW
Rated Reactive Power	Q_i^*	10KVAr
P-$\dot{V}$ Droop Coeff.	$m_i = \frac{1}{D_{pi}}$	$1.6 \cdot 10^{-3}\ \frac{V}{W \cdot s}$
Q-ω Droop Coeff.	$n_i = \frac{1}{D_{qi}}$	$3.1416 \cdot 10^{-4}\ \frac{rad}{Var \cdot s}$
ETRM parameters	k_{pr}, k_{qr} λ	1000 800
SETM parameters	η_{pi} η_{qi}	193.442 7.8957
DETM parameters	α_{pi}, α_{qi} β_{pi}, β_{qi} γ_{pi}, γ_{qi}	0.95 1 1

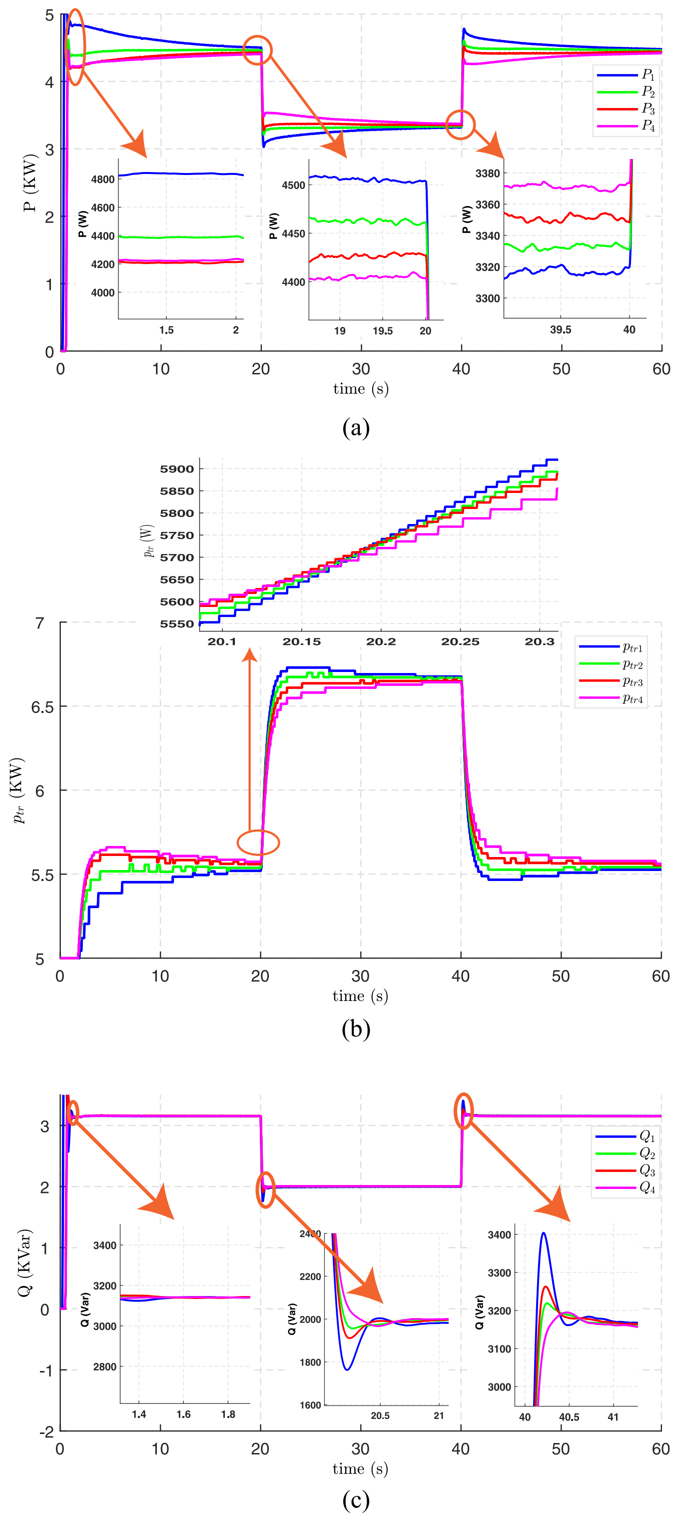

Fig. 6. Regulation process of the DGs under ETSM with SETM. (a) Active power $P(t)$. (b) Restoration variable $p_i(t)$ transmitted to its neighbors at triggering instants, i.e., $p_i(t_g^i)$. (c) Reactive power $Q(t)$.

droop method, the sharing accuracy of P has been improved by nearly 10%. However, it is hard to improve the power sharing accuracy further, since only bounded stability is available under ETSM with SETM as pointed out by Theorem 1.

The restoration variable $p_i(t)$ transmitted to its neighbours at triggering instants, i.e., $p_i(t_g^i)$, is shown as Fig. 6(b).

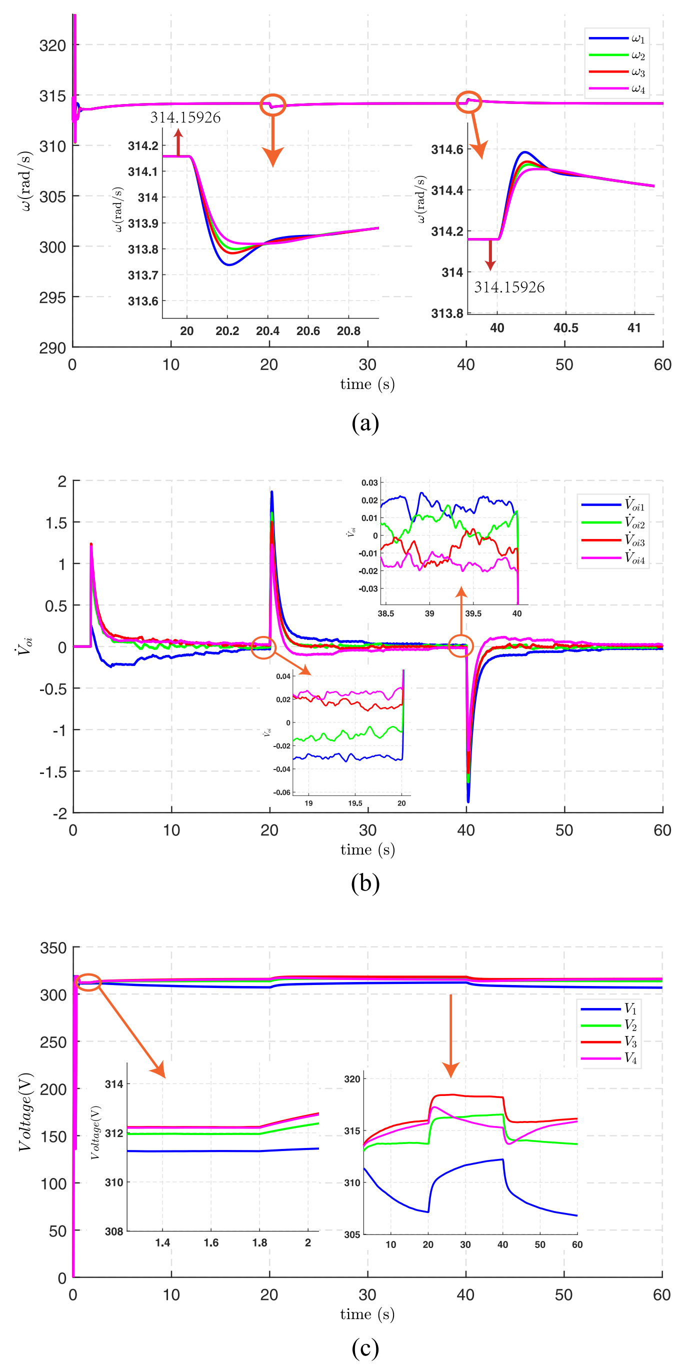

Fig. 7. Regulation process of the DGs under the ETSM with SETM. (a) Angular frequency $\omega(t)$. (b) Changing rate of voltage magnitude reference $\dot{V}_{oi}(t)$. (c) Voltage magnitude V.

It should be noted that the discrete triggering sequences $\{p_i(t_0^i), p_i(t_1^i), \ldots, p_i(t_g^i), \ldots\}$ are some discrete points. They are connected through ZOH and are renamed as p_{tr} for distinction. As mentioned in Remark 4, there exists a tradeoff between the power sharing accuracy and triggering rate. Since the former is preferred in this study, the value of η_{pi} cannot be large. Therefore, the triggering frequency is enlarged at the initial regulation process when the load changes, for example, $t \in [20.1, 20.3]$ s, as shown at the top of Fig. 6(b). More specific analysis is presented in Section V-B and is thus omitted here.

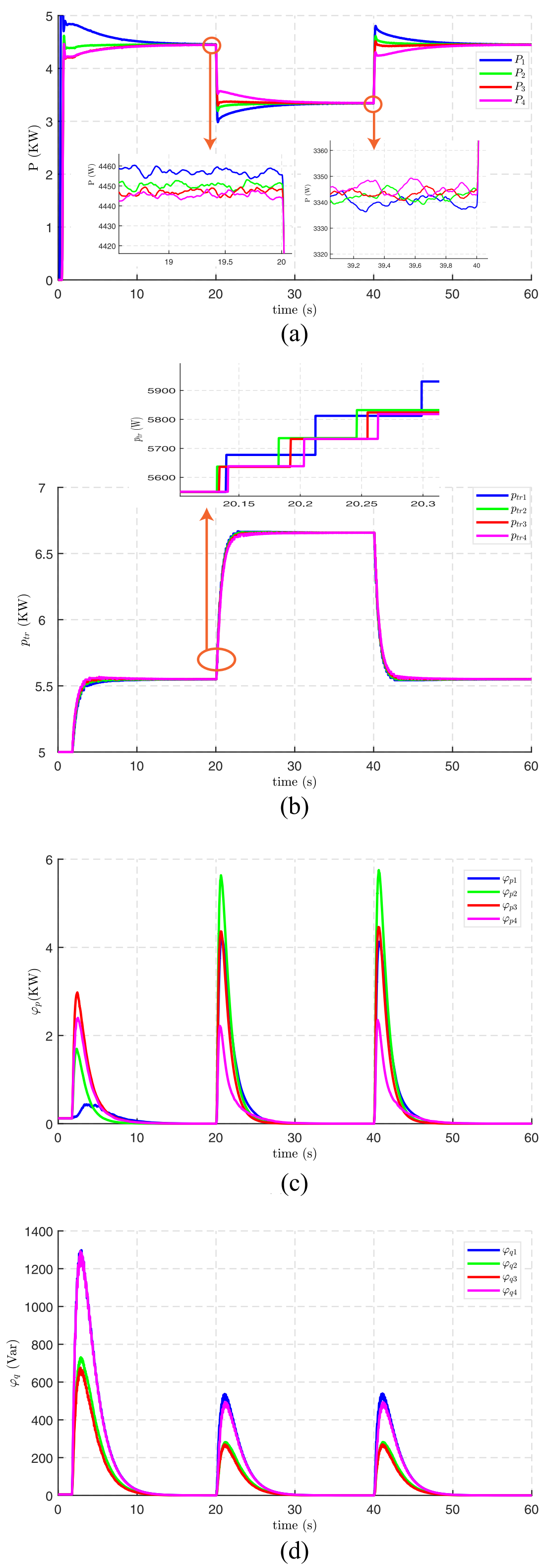

Fig. 8. Regulation process of the DGs under the ETSM with DETM. (a) Active power $P(t)$. (b) Restoration variable $p_i(t)$ transmitted to its neighbors at triggering instants. (c) Internal dynamic variable $\varphi_{pi}(t)$. (d) Internal dynamic variable $\varphi_{qi}(t)$.

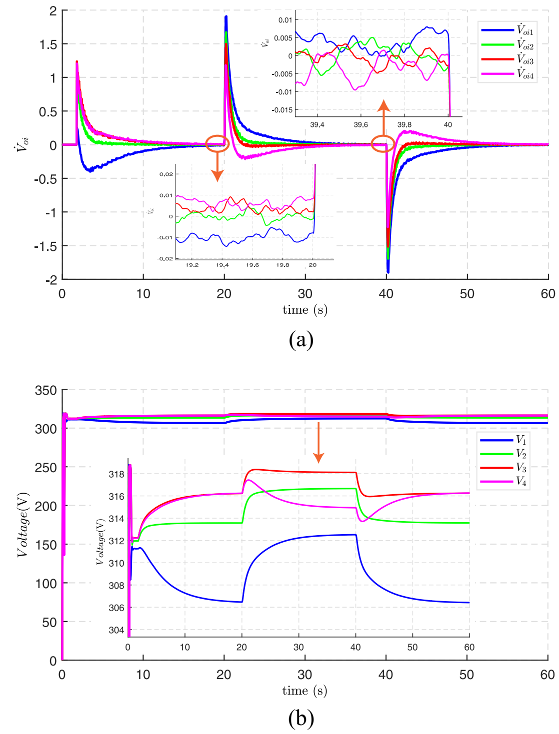

Fig. 9. Regulation process of the DGs under the ETSM with DETM. (a) Changing rate of voltage magnitude reference $\dot{V}_{oi}(t)$. (b) Voltage magnitude V.

In the traditional $P{-}f/Q{-}\omega$ droop method, the proportional sharing of active power can be achieved due to the negative feedback regulation of the global quantity ω. With a similar analysis, the fair sharing of reactive power Q under the $P - \dot{V}/Q - \omega$ droop method can be achieved and is illustrated in Fig. 6(c) during $t \in [1.5, 1.8]$ s. Besides, Fig. 6(c) also indicates that the reactive power Q is fairly shared during the regulation process except for the transient process after the load changes.

The angular frequency ω of DGs deviates from its nominal value under the $P - V/Q - \omega$ droop method as shown in Fig. 7(a) during $t < 1.8$ s. After the ETSM with SETM is activated, ω_i is restored to a tiny neighborhood around its rated value. Fig. 7(b) and (c) indicates that the improved sharing accuracy of P is achieved at the cost of larger voltage magnitude difference. Nevertheless, the required voltage level that $|V_i - V^*| = |V_i - 311| < 15V = 5\%V^*$ is fulfilled during the regulation process as shown in Fig. 7(c). At the steady state, $|\dot{V}_{oi}|$ is bounded to 0.02 as shown in Fig. 7(b). Thus, only bounded stability is available, since the voltage magnitudes of DGs will fluctuate in a tiny range. The triggering information is analyzed in Section V-D and is thus omitted here.

B. Case Study: Dynamic Event-Triggered Mechanism

In Section V-A, the fair utilization of Q and restoration of ω have been realized. In this section, the above conclusion holds true. Thus, some relative figures are omitted due to the limit of pages.

As shown in Fig. 8(a), the active power injections of DGs at $t = 20$ s are $P_1 = 4456$ W, $P_2 = 4451$ W, $P_3 = 4448$ W, and $P_4 = 4444$ W. The worst utilization ratio of DGs is $(P_4/P_1)|_{t=20\text{ s}} = 99.73\%$. At $t = 40$ s, we have $(P_1/P_2)|_{t=40\text{ s}} = 99.79\%$. Therefore, we can conclude that accurate fair utilization of P is achieved under the ETSM with DETM, which corresponds with Theorem 3.

Remark 7: It only takes half the time for the system under the DETM entering the steady state compared with that under the SETM in this study. Thus, the DETM outperforms the SETM in both transient regulation speed and steady sharing accuracy.

Similar to Fig. 6(b), the transmitted restoration variable p_{tr} is presented in Fig. 8(b). During $t \in [20.1,\ 20.3]$ s, the number of step change of p_{tr} is much smaller than that of Fig. 6(b). Thus, the triggering frequency of the DETM is much smaller than that of the SETM during the transient regulation process. Besides, the difference between p_{tr} of Fig. 8(b) is larger than that of Fig. 6(b), which corresponds with Remark 6.

Fig. 8(c) and (d) provides the regulation of internal dynamic variable φ_{pi} and φ_{qi}. Both φ_{pi} and φ_{qi} are not negative during the regulation process. When the load changes, they are adaptively regulated to a large value to reduce the triggering frequency, and then gradually converge to zero at the steady state.

At the steady state, all $|\dot{V}_{oi}|$ are bounded to 0.01 under DETM as shown in Fig. 9(a), which is only half of that of SETM. Fig. 9(b) is slightly different from Fig. 7(c). Thus, the operation code of voltage magnitude is also fulfilled in this case.

C. Case Study: Periodic Time-Triggered Mechanism

In this section, the performance of the PTTM is compared to that of the proposed SETM and DETM. The detailed formulation of the PTTM preferred in this research is shown as

$$k_{pi}\dot{p}_i(t) = P_i^* - P_i(t) - p_i(t) + \lambda \sum_{j\in N_i}\left(\frac{p_j(t)}{D_{pj}} - \frac{p_i(t)}{D_{pi}}\right)$$
$$k_{qi}\dot{q}_i(t) = Q_i^* - Q_i(t) - q_i(t) + \lambda \sum_{j\in N_i}\left(\frac{q_j(t)}{D_{qj}} - \frac{q_i(t)}{D_{qi}}\right). \tag{14}$$

As shown in Fig. 10(a), the regulation process is similar with that of the DETM. The active power injections of DGs at $t = 20$ s are $P_1 = 4456$ W, $P_2 = 4450$ W, $P_3 = 4446$ W, $P_4 = 4446$ W while $P_1 = 3344$ W, $P_2 = 3339$ W, $P_3 = 3343$ W, $P_4 = 3345$ W at $t = 40$ s. The worst utilization ratios of DGs are $(P_4/P_1)|_{t=20\,s} = 99.78\%$ and $(P_2/P_4)|_{t=40\,s} = 99.82\%$, which are almost equal to the ratios under the DETM. Therefore, the active power sharing accuracy and transient performance of PTTM are similar to that of the DETM.

Compared with the varying triggering period of the SETM and DETM, the triggering period of the PTTM is constant and is selected to be the sampling period, i.e., 0.05 ms, in this study. This tiny period means that the variation of p_{tri} can be seen as continuous during $t \in [20.1,\ 20.3]$ s, as shown in Fig. 10(b).

Therefore, the local data are transmitted to its neighbors regardless of the system state under the PTTM, which leads to a heavy pressure on the CI, while little improvement is achieved compared with that of the DETM.

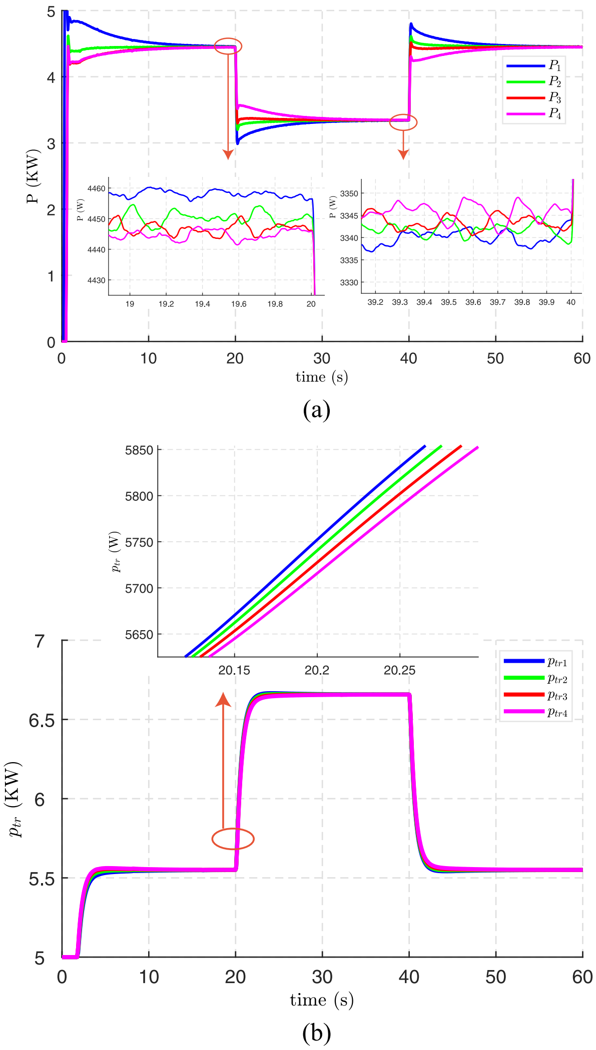

Fig. 10. Regulation process of the DGs under the PTTM. (a) Active power $P(t)$. (b) Restoration variable $p_i(t)$ transmitted to its neighbors at triggering instants.

D. Analysis of the Broadcast Period

The realization of purposes 1, 2 and 4, 5 has been discussed in Sections V-A and V-B. With the introduction of the ETM, the adjacent triggering time intervals or broadcast period is an outstanding indicator whether the communication burden has been reduced or not. In other words, the fulfilment of purpose 3 is demonstrated in this section. Due to the page limit, only the broadcast period of p_1 under the SETM and DETM is presented.

The total triggering times of Fig. 11 is 152, and most of the triggering instants gather at the start of load variation. In the steady state, few triggering events happen due to the incorporation of the static quantity η_{p1}. The minimum broadcast period is 5 ms, and thus the Zeno behavior is avoided as verified by Theorem 2.

According to Fig. 12, the total triggering times is 222 and are distributed during the time interval $t \in [1.8$ s, 60 s$]$. When the load changes, the triggering frequency of the DETM is

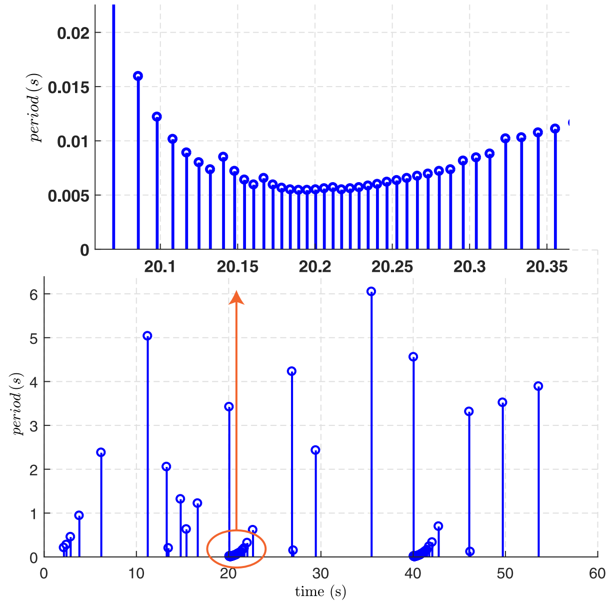

Fig. 11. Broadcast period of p_1 under SETM.

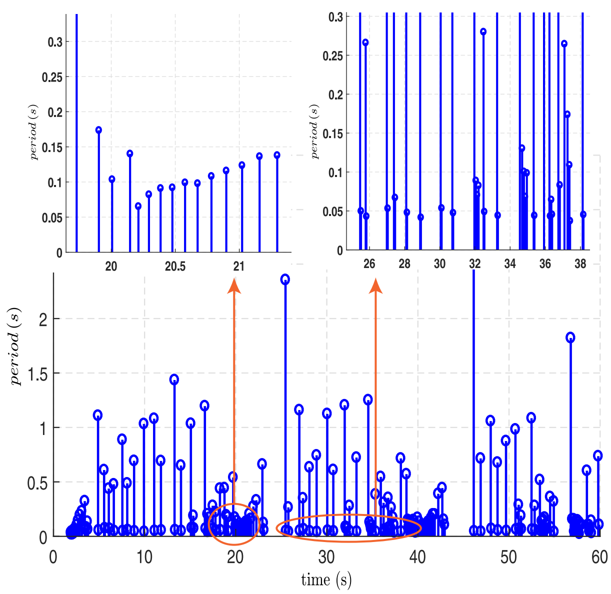

Fig. 12. Broadcast period of p_1 under DETM.

only one twentieth of the SETM, due to the dynamic variation of φ_{p1}. In the steady state, φ_{p1} is reset to zero, and thus the triggering condition (11) is easier to be reached, which is the root cause that more frequent triggering events happen at the steady state. Nevertheless, the minimum broadcast period of the DETM is 50 ms, and thus the Zeno behavior is excluded as verified by Theorem 4.

Since the minimum triggering period of the DETM is ten times larger than that of the SETM, the former is easier to be implemented in practical applications.

VI. Conclusion

In this article, we have examined the problem of frequency restoration and power sharing accuracy of the LVMG. The resistive nature of the LVMG is considered and the equivalent output impedance is constructed to be resistive with the virtual complex impedance strategy. A $P - \dot{V}/Q - \omega$ droop method is adopted to stabilize the system [25]. Then, an ETSM is designed to restore the frequency and improve the power sharing accuracy. Both SETM and DETM are proposed to determine the triggering time sequences.

With the theoretical analysis and simulation results, we have come to the following conclusion.

1) Compared with the $P-\dot{V}/Q-\omega$ droop method [25], both the proposed SETM and DETM are able to restore the frequency to its nominal value and improve the power sharing accuracy. Bounded stability of the system is ensured under the SETM with the ETSM, while the system is asymptotically stable under the DETM with the ETSM. In both cases, Zeno behavior is excluded.
2) Compared with the method mentioned in [22], the proposed methods can be seen as a general form of the former.
3) Compared with the PTTM, the proposed methods are more realistic due to the lower requirement on the CI owing to the adoption of ETM.
4) The total triggering events of the SETM are much less than that of the DETM and the former is easier to be implemented. However, the minimum triggering period of the DETM is much larger than that of the SETM. Besides, the DETM outperforms the SETM in both transient regulation speed and steady sharing accuracy. Therefore, the adoption of either should cater for the application scenario.

Our future work will concentrate on the combination of the finite-time control concept and the ETM. With the finite-time control scheme, the convergence speed of the ETSM can be accelerated to adapt to the dynamic variation of the loads. Besides, with the increasing concerns of cyber attacks on MGs, it is urgent to explore resilient controllers to cope with different types of cyber attacks [32]–[34].

References

[1] A. Bidram and A. Davoudi, “Hierarchical structure of microgrids control system,” *IEEE Trans. Smart Grid*, vol. 3, no. 4, pp. 1963–1976, Dec. 2012.

[2] B. Zhang, C. Dou, D. Yue, Z. Zhang, and T. Zhang, “A packet loss-dependent event-triggered cyber-physical cooperative control strategy for islanded microgrid,” *IEEE Trans. Cybern.*, early access, Dec. 13, 2019, doi: 10.1109/TCYB.2019.2954181.

[3] B. Liu, Z. Liu, J. Liu, R. An, H. Zheng, and Y. Shi, “An adaptive virtual impedance control scheme based on small-ac-signal injection for unbalanced and harmonic power sharing in islanded microgrids,” *IEEE Trans. Power Electron.*, vol. 34, no. 12, pp. 12333–12355, Dec. 2019.

[4] X. Meng, J. Liu, and Z. Liu, “A generalized droop control for grid-supporting inverter based on comparison between traditional droop control and virtual synchronous generator control,” *IEEE Trans. Power Electron.*, vol. 34, no. 6, pp. 5416–5438, Jun. 2019.

[5] F. Mohammadi, G.-A. Nazri, and M. Saif, “An improved droop-based control strategy for MT-HVDC systems,” *Electronics*, vol. 9, no. 1, p. 87, 2020.

[6] Y. Han, H. Li, P. Shen, E. A. A. Coelho, and J. M. Guerrero, “Review of active and reactive power sharing strategies in hierarchical controlled microgrids,” *IEEE Trans. Power Electron.*, vol. 32, no. 3, pp. 2427–2451, Mar. 2017.

[7] M. Savaghebi, A. Jalilian, J. C. Vasquez, and J. M. Guerrero, "Secondary control scheme for voltage unbalance compensation in an islanded droop-controlled microgrid," *IEEE Trans. Smart Grid*, vol. 3, no. 2, pp. 797–807, Jun. 2012.

[8] Y. Guan, J. C. Vasquez, and J. M. Guerrero, "Coordinated secondary control for balanced discharge rate of energy storage system in islanded AC microgrids," *IEEE Trans. Ind. Appl.*, vol. 52, no. 6, pp. 5019–5028, Nov./Dec. 2016.

[9] Y. Han, H. Li, L. Xu, X. Zhao, and J. M. Guerrero, "Analysis of washout filter-based power sharing strategy—An equivalent secondary controller for islanded microgrid without LBC lines," *IEEE Trans. Smart Grid*, vol. 9, no. 5, pp. 4061–4076, Sep. 2018.

[10] J. Lu, M. Savaghebi, and J. M. Guerrero, "Second order washout filter based power sharing strategy for uninterruptible power supply," in *Proc. IEEE 43rd Annu. Conf. Ind. Electron. Soc. (IECON)*, Beijing, China, 2017, pp. 7854–7859.

[11] A. Bidram, A. Davoudi, F. L. Lewis, and Z. Qu, "Secondary control of microgrids based on distributed cooperative control of multi-agent systems," *IET Gener. Transm. Distrib.*, vol. 7, no. 8, pp. 822–831, Aug. 2013.

[12] F. Guo, C. Wen, J. Mao, and Y. Song, "Distributed secondary voltage and frequency restoration control of droop-controlled inverter-based microgrids," *IEEE Trans. Ind. Electron.*, vol. 62, no. 7, pp. 4355–4364, Jul. 2015.

[13] J. W. Simpson-Porco, Q. Shafiee, F. Dörfler, J. C. Vasquez, J. M. Guerrero, and F. Bullo, "Secondary frequency and voltage control of islanded microgrids via distributed averaging," *IEEE Trans. Ind. Electron.*, vol. 62, no. 11, pp. 7025–7038, Nov. 2015.

[14] R. Han, L. Meng, G. Ferrari-Trecate, E. A. A. Coelho, J. C. Vasquez, and J. M. Guerrero, "Containment and consensus-based distributed coordination control to achieve bounded voltage and precise reactive power sharing in islanded AC microgrids," *IEEE Trans. Ind. Appl.*, vol. 53, no. 6, pp. 5187–5199, Nov./Dec. 2017.

[15] X. Lu, X. Yu, J. Lai, Y. Wang, and J. M. Guerrero, "A novel distributed secondary coordination control approach for islanded microgrids," *IEEE Trans. Smart Grid*, vol. 9, no. 4, pp. 2726–2740, Jul. 2018.

[16] Q. Li, C. Peng, M. Wang, M. Chen, J. M. Guerrero, and D. Abbott, "Distributed secondary control and management of islanded microgrids via dynamic weights," *IEEE Trans. Smart Grid*, vol. 10, no. 2, pp. 2196–2207, Mar. 2019.

[17] Y. Khayat *et al.*, "On the secondary control architectures of AC microgrids: An overview," *IEEE Trans. Power Electron.*, vol. 35, no. 6, pp. 6482–6500, Jun. 2020.

[18] L. Ding, Q. Han, X. Ge, and X. Zhang, "An overview of recent advances in event-triggered consensus of multiagent systems," *IEEE Trans. Cybern.*, vol. 48, no. 4, pp. 1110–1123, Apr. 2018.

[19] C. Peng, S. Ma, and X. Xie, "Observer-based non-PDC control for networked T–S fuzzy systems with an event-triggered communication," *IEEE Trans. Cybern.*, vol. 47, no. 8, pp. 2279–2287, Aug. 2017.

[20] X. Zhang *et al.*, "Networked control systems: A survey of trends and techniques," *IEEE/CAA J. Autom. Sinica*, vol. 7, no. 1, pp. 1–17, Jan. 2020.

[21] C. Yang *et al.,* "Dynamic event-triggered robust secondary frequency control for islanded AC microgrid," *Appl. Energy*, vol. 242, pp. 821–836, May 2019.

[22] S. Weng, D. Yue, C. Dou, J. Shi, and C. Huang, "Distributed event-triggered cooperative control for frequency and voltage stability and power sharing in isolated inverter-based microgrid," *IEEE Trans. Cybern.*, vol. 49, no. 4, pp. 1427–1439, Apr. 2019.

[23] L. Ding, Q. Han, and X. Zhang, "Distributed secondary control for active power sharing and frequency regulation in islanded microgrids using an event-triggered communication mechanism," *IEEE Trans. Ind. Informat.*, vol. 15, no. 7, pp. 3910–3922, Jul. 2019.

[24] J. Saroha, M. Singh, and D. K. Jain, "ANFIS-based add-on controller for unbalance voltage compensation in a low-voltage microgrid," *IEEE Trans. Ind. Informat.*, vol. 14, no. 12, pp. 5338–5345, Dec. 2018.

[25] J. Chen, D. Yue, C. Dou, L. Chen, S. Weng, and Y. Li, "A virtual complex impedance based $P-\dot{V}$ droop method for parallel-connected inverters in low-voltage AC microgrids," *IEEE Trans. Ind. Informat.*, early access, May 25, 2020, doi: 10.1109/TII.2020.2997054.

[26] J. M. Guerrero, J. C. Vasquez, J. Matas, L. G. de Vicuna, and M. Castilla, "Hierarchical control of droop-controlled AC and DC microgrids—A general approach toward standardization," *IEEE Trans. Ind. Electron.*, vol. 58, no. 1, pp. 158–172, Jan. 2011.

[27] X. Wang, F. Blaabjerg, Z. Chen, and W. Wu, "Resonance analysis in parallel voltage-controlled distributed generation inverters," in *Proc. 28th Annu. IEEE Appl. Power Electron. Conf. Exposit. (APEC)*, Long Beach, CA, USA, 2013, pp. 2977–2983.

[28] C. Lee, C. Chu, and P. Cheng, "A new droop control method for the autonomous operation of distributed energy resource interface converters," *IEEE Trans. Power Electron.*, vol. 28, no. 4, pp. 1980–1993, Apr. 2013.

[29] J. Zhou and P. Cheng, "A modified $Q-\dot{V}$ droop control for accurate reactive power sharing in distributed generation microgrid," *IEEE Trans. Ind. Appl.*, vol. 55, no. 4, pp. 4100–4109, Jul. 2019.

[30] L. Lu and C. Chu, "Consensus-based droop control synthesis for multiple DICs in isolated micro-grids," *IEEE Trans. Power Syst.*, vol. 30, no. 5, pp. 2243–2256, Sep. 2015.

[31] L. Q. Thuan and M. K. Camlibel, "Continuous piecewise affine dynamical systems do not exhibit zeno behavior," *IEEE Trans. Autom. Control*, vol. 56, no. 8, pp. 1932–1936, Aug. 2011.

[32] S. Hu, D. Yue, X. Xie, X. Chen, and X. Yin, "Resilient event-triggered controller synthesis of networked control systems under periodic DoS jamming attacks," *IEEE Trans. Cybern.*, vol. 49, no. 12, pp. 4271–4281, Dec. 2019.

[33] W. Ao, Y. Song, and C. Wen, "Distributed secure state estimation and control for CPSs under sensor attacks," *IEEE Trans. Cybern.*, vol. 50, no. 1, pp. 259–269, Jan. 2020.

[34] Y. Wan, C. Long, R. Deng, G. Wen, X. Yu, and T. Huang, "Distributed event-based control for thermostatically controlled loads under hybrid cyber attacks," *IEEE Trans. Cybern.*, early access, Mar. 23, 2020, doi: 10.1109/TCYB.2020.2978274.

Jianbo Chen (Graduate Student Member, IEEE) received the B.S. degree in electrical engineering and automation from Nanjing University of Posts and Telecommunications, Nanjing, China, in 2015, where he is currently pursing the Ph.D. degree.

His current research interests include distributed control, event-triggered control, parallel control of multiple inverters, and the power quality improvement of the microgrid.

Dong Yue (Senior Member, IEEE) received the Ph.D. degree from the South China University of Technology, Guangzhou, China, in 1995.

He is currently a Professor and the Dean of the Institute of Advanced Technology and College of Automation and AI, Nanjing University of Posts and Telecommunications, Nanjing, China. Up to now, he has published more than 250 papers in international journals and two books. He holds more than 50 patents. His research interests include analysis and synthesis of networked control systems, multiagent systems, optimal control of power systems, and Internet of Things.

Prof. Yue has served as an Associate Editor of *IEEE Industrial Electronics Magazine*, IEEE TRANSACTIONS ON INDUSTRIAL INFORMATICS, IEEE TRANSACTIONS ON SYSTEMS, MAN, AND CYBERNETICS: SYSTEMS, IEEE TRANSACTIONS ON NEURAL NETWORKS AND LEARNING SYSTEMS, *Journal of the Franklin Institute*, and *International Journal of Systems Sciences*, the Guest Editor of Special Issue on New Trends in Energy Internet: Artificial Intelligence-Based Control, Network Security and Management, and IEEE TRANSACTIONS ON SYSTEMS, MAN, AND CYBERNETICS: SYSTEMS.

Chunxia Dou (Member, IEEE) received the B.S. and M.S. degrees in automation from Northeast Heavy Machinery Institute, Qiqihaer, China, in 1989 and 1994, respectively, and the Ph.D. degree in measurement technology and instrumentation from the Institute of Electrical Engineering, Yanshan University, Qinhuangdao, China, in 2005.

In 2010, she joined the Department of Engineering, Peking University, Beijing, China, where she was a Postdoctoral Fellow for two years. Since 2005, she has been a Professor with the Institute of Electrical Engineering, Yanshan University, and a Professor of the Institute of Advanced Technology, Nanjing University of Posts and Telecommunications, Nanjing, China. Her current research interests include multiagent-based control, event-triggered hybrid control, distributed coordinated control, and multimode switching control and their applications in power systems, microgrids, and smart grids.

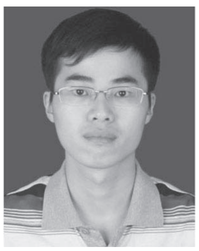

Shengxuan Weng received the B.S. degree from the School of Mathematics and Statistics, Huazhong University of Science and Technology, Wuhan, China, in 2009, and the Ph.D. degree from the School of Automation, Huazhong University of Science and Technology in 2014.

Since 2014, he has been with the Institute of Advanced Technology, Nanjing University of Posts and Telecommunications, Nanjing, China. His current research interests include distributed control, multiagent system, and control approach in microgrid and smart grid.

Xiangpeng Xie (Member, IEEE) received the B.S. and Ph.D. degrees in engineering from Northeastern University, Shenyang, China, in 2004 and 2010, respectively.

From 2010 to 2014, he was a Senior Engineer with the Metallurgical Corporation of China Ltd., Beijing, China. He is currently a Professor with the Institute of Advanced Technology, Nanjing University of Posts and Telecommunications, Nanjing, China. His research interests include fuzzy modeling and control synthesis, state estimations, optimization in process industries, and intelligent optimization algorithms.

Prof. Xie serves as an Associate Editor for the *International Journal of Fuzzy Systems* and *International Journal of Control, Automation, and Systems*.

Yanman Li received the M.S. degree in cartography and geographic information system from Nanjing University, Nanjing, China, in 1996 and 1999, respectively.

He works with the State Grid Electric Power Research Institute, Nanjing, as an Associate Professor Level Senior Engineer. His research interests include distribution automation, active distribution network, and electric power automatic information system.

Gerhard P. Hancke (Life Fellow, IEEE) received the B.Sc., B.Eng., and M.Eng. degrees in electronic engineering from the University of Stellenbosch, Stellenbosch, South Africa, in 1970 and 1973, respectively, and the D.Eng. degree from the University of Pretoria, Pretoria, South Africa, in 1983.

He is a Professor with the Nanjing University of Posts and Telecommunications, Nanjing, China, and the University of Pretoria. He is recognized internationally as a pioneer and leading scholar in Industrial Wireless Sensor Networks Research. He initiated and co-edited the first Special Section on Industrial Wireless Sensor Networks in the IEEE Transactions on Industrial Electronics in 2009 and the IEEE Transactions on Industrial Informatics in 2013. He co-edited a textbook, *Industrial Wireless Sensor Networks: Applications, Protocols and Standards*, in 2013, the first on the topic.

Prof. Hancke has been serving as an Associate Editor and a Guest Editor for the IEEE Transactions on Industrial Informatics, IEEE Access, and the IEEE Transactions on Industrial Electronics. He is currently the Co-Editor-in-Chief of the IEEE Transactions on Industrial Informatics and a Senior Editor of IEEE Access.